ENGINEERING APPLICATIONS OF COMPUTATIONAL FLUID MECHANICS, 2017
VOL. 11, NO. 1, 142–158
http://dx.doi.org/10.1080/19942060.2016.1247297

Taylor & Francis
Taylor & Francis Group

Comparison of the effects of surface roughness and confinement on rotor–stator cavity flow

M. Özkan [a], P. J. Thomas[a], A. J. Cooper[a] and S. J. Garrett[b]

[a]School of Engineering, University of Warwick, Coventry, UK; [b]Department of Engineering, University of Leicester, Leicester, UK

ABSTRACT

Results of a computational study are discussed which investigate roughness-induced and geometry-induced (confinement) effects on the steady-state velocity components in 3-D boundary-layer flow over the rotor disc in a rotor–stator flow configuration. It is found that, for the rotor–stator flow investigated, the roughness-induced effects are very similar to geometry-induced effects, both in nature and magnitude. The overall aim was to compare these two types of effects with corresponding roughness-induced effects in the von Kármán boundary-layer flow over a disc spinning freely in an unrestricted fluid environment. The research was conducted in the context of a programme investigating surface roughness as a means of laminar flow control for the development of new passive drag-reduction techniques. The goal was to establish whether it was possible unequivocally to distinguish between roughness-induced and geometry-induced effects on the boundary-layer flow above the rotor disc. The results obtained suggest that, for the type of system discussed here, it must be expected to be difficult to distinguish between these effects in experiments. The similarities regarding the nature and magnitude of results obtained from comparing predictions for three different computational modelling approaches indicate the required sensitivity of measurement technologies aiming to resolve the investigated effects in experimental studies.

ARTICLE HISTORY
Received 3 February 2016
Accepted 8 October 2016

KEYWORDS
laminar flow control; drag reduction; rotor–stator flow; rotating-disc flow; boundary-layer transition; rough walls

1. Introduction

Rotor–stator cavity flow is a generic flow configuration encountered in a wide variety of problems of applied engineering interest. Generally, rotor–stator flow is the flow established within the confined, fluid-filled volume between a rotating disc and an annular, stationary enclosure as illustrated in Figure 1. Reviews of the subject and the available relevant literature are provided by Owen and Rogers (1989), Launder et al. (2010) and the references cited therein.

The flow over the rotor of Figure 1 in the case when the stator is absent represents the flow over a rotating disc in an unrestricted, infinite fluid environment. In the general context of rotating-disc flow one distinguishes between three different scenarios. These are the cases (cf. Lingwood & Alfredsson, 2015) of stationary fluid above a rotating disc (von Kármán flow), a rotating fluid above a stationary disc (Bödewadt flow) and the case where both the disc and the fluid rotate at approximately equal rates (Ekman flow). These three scenarios are commonly referred to as the Bödewadt–Ekman–von Kármán (BEK) family of flows.

Rotor–stator flow gives rise to a boundary layer on the rotor disc. The rotor drives a recirculating secondary flow motion within the cavity between the rotor and the stator. As a result, a boundary layer also forms on the stator. Consequently, there exists a swirling core-flow region between the two opposing boundary layers. Thus, rotor–stator flow combines aspects of von Kármán flow, Bödewadt flow and Ekman flow.

The current study compares computational results for effects arising from the presence of roughness on the surface of the rotor disc with effects arising from the diameter-to-height aspect ratio associated with the cavity between the rotor disc and the stator. The main focus of the study is on the steady-state, base-flow profiles which are required for a subsequent stability analysis of the boundary layer established over the rotor disc. However, a brief comment regarding the stability of the boundary layer on the rotor disc is included since an aspect obtained from stability calculations based on the results discussed here bears close relevance to results on BEK flows recently reported by Alveroglu, Segalini and Garrett (2016).

CONTACT M. Özkan musa.zkan@gmail.com; P. J. Thomas P.J.Thomas@warwick.ac.uk

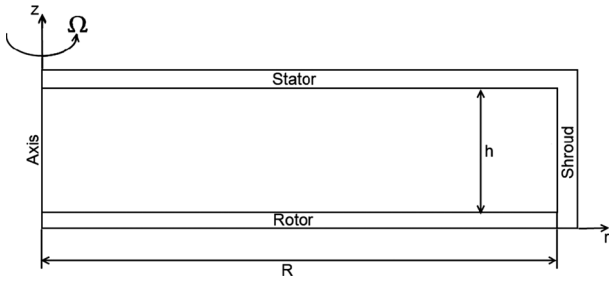

Figure 1. A sketch of an enclosed rotor–stator cavity.

Rotating-disc flow of von Kármán type constitutes the paradigm flow configuration employed for the study of fully three-dimensional boundary layers with a cross-flow component. Such boundary layers are encountered in similar form in, for instance, the flow over the blades of wind turbines or highly-swept wings (Lingwood & Alfredsson, 2015; Reed & Saric, 1989; Saric et al., 2003). Here we address the rotating-disc flow in a rotor–stator arrangement in the context of an issue that first arose in connection with some of the research on the laminar–turbulent transition of rotating-disc boundary-layer flow over compliant surfaces in Colley, Thomas, Carpenter and Cooper (1999) and Colley, Carpenter, Thomas, Ali, and Zoueshtiagh (2006) and which has now become of relevance again in association with the interpretation of results from some of the latest research on the effects of surface roughness on the transition process over a rotating disc in Cooper, Harris, Garrett, Özkan, and Thomas (2015) and Garrett et al. (2016). These two studies address roughness effects with the long-term goal of developing a theory-led approach to designing energetically optimal roughness, which delays the onset of laminar–turbulent boundary-layer transition, for new passive-drag reduction techniques.

The von Kármán case, i.e. flow where the fluid is at rest sufficiently far above the disc, is illustrated schematically in Figure 2. Due to the no-slip condition on the disc surface the disc drives an azimuthal, rotary flow in which centrifugal effects establish a flow component orientated radially outwards which, in turn, necessitates a downward, axial flow component towards the disc surface to satisfy continuity. For the case of a rotating disc, it is the radial flow component that represents the cross-flow component. The velocity profile of the cross-flow component has an inflection point at some height above the disc (cf. Figure 2) and this characteristic is shared by the cross-flow velocity profile of all other boundary layers where such a cross flow exists.

Boundary layers with an inflection point are prone to instability due to Rayleigh's inflection-point criterion (Schlichting & Gersten, 2004, p. 432). As a consequence, all boundary-layer flows with a cross-flow component display similar laminar–turbulent transition characteristics associated with the instability arising from the inflection point on the cross-flow velocity profile. Due to the similarities in the transition scenario for all boundary layers with a cross-flow component, rotating-disc flow has become the foremost example to study the transition process for this type of boundary layers because it is an easily accessible experimental configuration and because there exists an exact similarity solution, derived by von Kármán (1921), to the Navier–Stokes equations for the laminar rotating-disc boundary-layer flow.

Colley et al. (1999, 2006) investigated the transition process of boundary-layer flow over a rotating disc submerged in an aqueous environment. In order to minimize undesirable boundary effects such as those arising, for instance, from waves on the liquid surface, the disc was covered with a static shroud. Hence, the flow configuration investigated was effectively the rotor–stator configuration shown here in Figure 1; but note that Colley et al. (2006) also contains data where the static shroud was removed for comparison. Nevertheless, the main questions addressed in Colley et al. (1999, 2006) were associated with transition over a disc spinning in an infinite fluid environment. The analysis of the hot-film data discussed in Colley et al. (1999, 2006) revealed that the azimuthal component of the flow velocity (cf. Figure 2) did not approach zero, for increasing distances above the disc surface. This should, however, have been the case on the basis of the theoretical velocity profiles derived by von Kármán (1921) for a disc spinning in an infinite environment that is at rest far above the disc. Colley et al. (2006) commented, in connection with the discussion of Figure 2(b) in that paper, that it was likely that this result arose due to residual rotary motion above the boundary layer over the disc. It was, nevertheless, not necessary to consider this observation any further in connection with the particular issues addressed there.

However, Cooper et al. (2015) and Garrett et al. (2016) began to investigate roughness effects on the transition process of the boundary-layer flow over a rotating disc. In order to become able to perform a linear stability analysis for the boundary-layer flow they had initially to determine the roughness-induced modifications to the steady-state base-flow velocity profiles of the rotating-disc boundary layer. One of the theoretical results obtained was that the roughness-induced effects on the azimuthal velocity profile for a disc spinning in an infinite fluid environment, which is at rest sufficiently far above the disc (von Kármán flow), bore resemblance to the experimentally obtained azimuthal velocity profiles reported in Colley et al. (1999, 2006) with its residual azimuthal flow. This triggered the question as

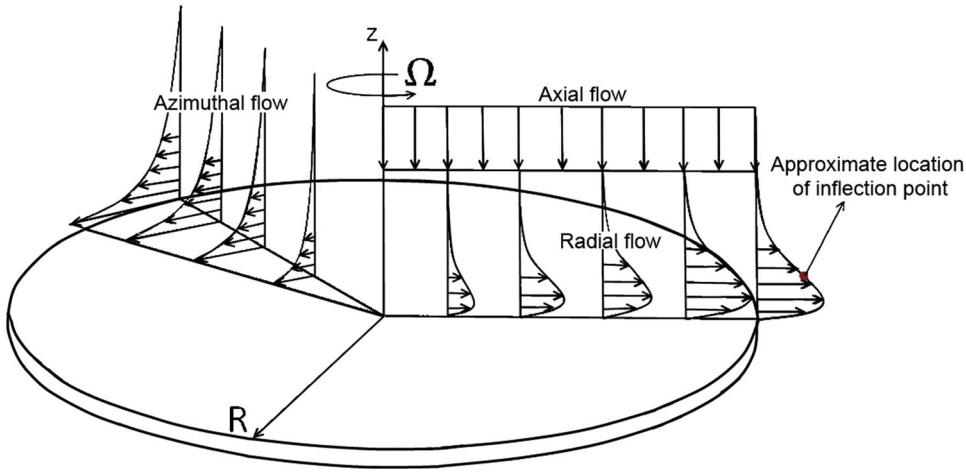

Figure 2. The three velocity components of rotating-disc flow.

to whether it would be possible, in general, always to unambiguously distinguish between roughness-induced and confinement-induced effects for rotating-disc and rotor–stator flow. The results described and discussed here represent the first investigation addressing this issue.

2. Problem formulation

2.1. The flow configuration

2.1.1. Rotor–stator flow

The sketch of the three-dimensional rotor–stator flow configuration examined is illustrated in Figure 1. The problem is described in a stationary, cylindrical polar-coordinate system z, θ, r. The rotor disc has radius R and it is spinning about the z-axis with an angular velocity Ω. The stator is enclosed by a stationary shroud with an internal radius equal to the disc radius. The volume between the rotor disc and the stator is filled with water at 20 °C where the kinematic viscosity of water is $\nu = 1.004\times10^{-6}\, m^2 s^{-1}$. The gap between the rotor and the stator has a height h such that the geometry is characterized by the aspect ratio $D = h/R$. A global rotational Reynolds number is defined as $\mathrm{Re}_\phi = \sqrt{\Omega R^2/\nu}$ to characterize the rotor–stator cavity flow. Note that we have introduced the root in the definition of the global Reynolds number to make the definition formally consistent with that of the local Reynolds number, to be introduced in the next section, normally used in connection with rotating-disc flow.

The global, recirculating flow induced by the rotor within the cavity results in the formation of boundary layers on both the rotor and the stator. The flow within the boundary layer of the rotor establishes a flow in which the radial component of the flow velocity is orientated away from the centre of the disc, as in Figure 2, whereas the flow in the boundary layer on the stator has the opposite orientation whereby the fluid flows towards the centre of the stator.

The motivating goal of the study is to compare the effects induced by the aspect ratio D, and by the surface roughness of the rotor disc, on the boundary-layer flow above the rotor disc with the effects which surface roughness induces on the flow in the boundary layer on a disc spinning in an infinite, unrestricted fluid environment.

2.1.2. Rotating-disc flow

In the limit $R \to \infty$ and $D \to \infty$, the rotor–stator flow configuration approaches the case of an infinite disc spinning in an unbounded fluid which is at rest sufficiently far above the disc. This limit of the flow configuration was first studied by von Kármán (1921), who derived an exact similarity solution to the Navier–Stokes equations for this flow. The solution yields the radial, azimuthal and axial components of the flow field (cf. Figure 2) which we refer to as, respectively, $u(z, r, \Omega)$, $v(z, r, \Omega)$ and $w(z, \Omega)$ – note that w is independent of the radial component r. The characteristic length scale relevant to the problem is given by $\delta^* = \sqrt{\nu/\Omega}$ which is used to non-dimensionalize the vertical coordinate as $\zeta = z/\delta^*$. The usual (local) rotational Reynolds number, corresponding to the non-dimensional radial distance from the centre of the disc, is defined as $\mathrm{Re} = \sqrt{\Omega r^2/\nu}$. The three components of the flow velocity are non-dimensionalized as

$$F(\zeta) = \frac{u}{\Omega r}, G(\zeta) = \frac{v}{\Omega r}, H(\zeta) = \frac{w}{\sqrt{\nu\Omega}} \qquad (1)$$

with boundary conditions $F(\zeta = 0) = 0$, $F(\zeta = \infty) = 0$, $G(\zeta = 0) = 1$, $G(\zeta = \infty) = 0$, $H(\zeta = 0) = 0$ and a value of $H(\zeta = \infty) = -0.8845$, the latter being obtained from a numerical solution of the von Kármán (1921) problem. A comprehensive set of numerical data for $F(\zeta)$,

$G(\zeta)$ and $H(\zeta)$, for $0 \leq \zeta \leq 10$, can be found in tabulated form in Table 3.1 in Owen and Rogers (1989, p. 47). Inspection of the data for $G(\zeta)$ in that table reveals that the boundary-layer thickness, i.e. the height for which the azimuthal velocity component is $v = 0.01\Omega r$ (that is, $G(\zeta) = 0.01$), is given by $\delta = 5.5\,\delta^*$.

2.2. Numerical model

The three-dimensional rotor–stator flow, and associated roughness effects, are simulated by means of the ANSYS® Fluent® software package implementing the Transition Shear-Stress-Transport model (hereinafter, the TSST model) based on Menter (1994) and Menter et al. (2006), and the full description and correlations of the model were reported by Langtry and Menter (2009). The choice of this transition model was motivated by our ongoing, concurrent investigations of issues associated with the transition process of the boundary-layer flow over the rotor disc. However, these results are not relevant in the context of the current study and, consequently, they are not discussed here. The suitability of the TSST model to perform simulations that include the effect of surface roughness has recently been demonstrated by Aldaş and Yapıcı (2014). They compared numerical results obtained on the basis of various turbulence models with experimental data and concluded that the TSST model provided the most accurate description of these.

The TSST model is based on empirical correlations and formed from the combination of the Shear-Stress-Transport (SST) k–ω model together with two additional transport equations for the intermittency γ and a transition onset criterion in terms of a momentum–thickness Reynolds number $\tilde{\mathrm{Re}}_{\Theta t}$. Here, $\tilde{\mathrm{Re}}_{\Theta t}$ is the Reynolds number formed using the local velocity U and the momentum–thickness δ_2. The definition of the momentum–thickness Reynolds number is given in Equation (2). The SST k–ω model by Menter (1994) can efficiently combine the robust and precise formulation of the k–ω model in the field close to a wall and the free-stream independence of the k–ε model in the region far from the wall.

$$\tilde{\mathrm{Re}}_{\Theta t} = \frac{U\delta_2}{\nu}. \tag{2}$$

The SST model solves continuity and momentum equations in conjunction with the transport equations for the turbulence kinetic energy k and the specific dissipation rate ω. The TSST model additionally solves the transport equations for the intermittency γ and the transition momentum–thickness Reynolds number $\tilde{\mathrm{Re}}_{\Theta t}$. The detailed coupling of the new TSST model with the SST turbulence model (Menter, 1994) can be found in Menter et al. (2006).

The intermittency γ characterizes the physical nature of the flow in terms of the fraction of time for which there exists turbulent flow at any specific location. The value $\gamma = 1$ indicates continuous turbulent flow, $\gamma = 0$ describes continuous laminar flow and values $0 < \gamma < 1$ characterize the transition region. The transport equation for the intermittency γ is defined as

$$\frac{\partial(\rho\gamma)}{\partial t} + \frac{\partial\left(\rho U_j \gamma\right)}{\partial x_j} = P_{\gamma 1} - E_{\gamma 1} + P_{\gamma 2} - E_{\gamma 2} + \frac{\partial}{\partial x_j}\left[\left(\mu + \frac{\mu_t}{\sigma_f}\right)\frac{\partial \gamma}{\partial x_j}\right], \tag{3}$$

where the detailed formulations of the transition sources $P_{\gamma 1}$ and $E_{\gamma 1}$ and the destruction/relaminarization sources $P_{\gamma 2}$ and $E_{\gamma 2}$ can be found in Menter et al. (2006).

The transport equation for the transition momentum–thickness Reynolds number $\tilde{\mathrm{Re}}_{\Theta t}$ is

$$\frac{\partial\left(\rho\tilde{\mathrm{Re}}_{\Theta t}\right)}{\partial t} + \frac{\partial\left(\rho U_j \tilde{\mathrm{Re}}_{\Theta t}\right)}{\partial x_j} = P_{\theta t} + \frac{\partial}{\partial x_j}\left[\sigma_{\theta t}\left(\mu + \mu_t\right)\frac{\partial \tilde{\mathrm{Re}}_{\Theta t}}{\partial x_j}\right], \tag{4}$$

where the source term $P_{\theta t}$ has the capability of forcing the transported scalar $\tilde{\mathrm{Re}}_{\Theta t}$ to correspond to the local value of $\mathrm{Re}_{\theta t}$ obtained from an experimental correlation.

A three-dimensional CFD model was created in Gambit® 2.1.6 where the fluid domain, water at 20 °C, filled the volume enclosed by the stator with its shroud (stationary walls) and the rotor (rotating wall) which drives the cavity flow inside the enclosure. A structured hexagonal mesh was produced by means of the same software and around 1,800,000 cells were generated to achieve mesh independent results. There are 20 cells inside the boundary layers of the rotor and the stator to provide sufficient resolution in these boundary layers. This mesh configuration also provides a y^+ of approximately one which is a crucial parameter to capture the laminar and transitional regions in the boundary layer (Langtry & Menter, 2009). The mesh model was then uploaded to Fluent® 15.0 and the double-precision pressure-based coupled algorithm was employed to solve the Reynolds-averaged Navier–Stokes equations. The simulations were conducted under pseudo transient conditions, which helps to avoid the possible divergence of the solution in consequence of high pressure gradients, especially during the early iterations. The least squares cell-based approach was used for gradient evaluation and second-order schemes were employed for spatial discretization. The iterations were stopped when the residuals of all equations dropped below a satisfactory value of 10^{-4}.

The roughness of the rotor-disc surface was defined in terms of a geometric roughness height K which was then transformed by the software into an equivalent sand-grain roughness height K_s. Thereafter the law-of-the-wall was modified for this roughness correspondingly. The reader is referred to page 75 of the ANSYS® (2013) Fluent® Theory Guide, and the cited references therein, for details of the modification of the law-of-the-wall and the transformation from the geometric roughness height K into the equivalent sand-grain roughness height K_s.

The results obtained by the TSST approach, for the case when the rotor disc is assumed to be smooth, are validated by comparison with the experimental data by Sambo (1983) with concurrent simulations by Vaughan (1986), experiments by Colley et al. (2006) and in comparison with the theoretical results by von Kármán (1921).

The effects predicted by the TSST approach to be arising from introducing surface roughness on the rotor disc are compared with corresponding results obtained on the basis of the methods described in Cooper et al. (2015), Garrett et al. (2016) and Alveroglu et al. (2016). There do not yet exist experimental data that could be used for a comparison with the predicted roughness effects. Obtaining such experimental data is one of the medium-term goals of our overall current research programme.

Unless stated otherwise the radius of the rotor–stator system for all TSST simulations is $R = 0.6\,m$ and the rotational velocity of the rotor disc is $\Omega = 1\,rad\,s^{-1}$, yielding a value of $\mathrm{Re}_\phi = 600$ for the global rotational Reynolds number.

3. Validation of the computational approach

Here, and in the remainder, only the azimuthal and radial flow components are considered because for the rotating-disc flow these are the dominant components governing the transition process of the boundary layer. The radial and azimuthal flow components are, moreover, an order of magnitude larger than the axial flow and one can normally only measure experimental data for these two flow components in rotating-disc boundary-layer experiments.

3.1. Comparison of TSST data for rotor–stator flow with numerical and experimental literature data

Figure 3 displays a comparison of computational results obtained from our TSST approach for the entire extent of the gap in the rotor–stator flow with its two opposing boundary layers on the rotor and the stator. The figure shows the radial and the azimuthal velocity components F and G, as a function of the height z/h above the rotor disc in comparison with numerical results of Vaughan (1986) and experimental data of Sambo (1983).

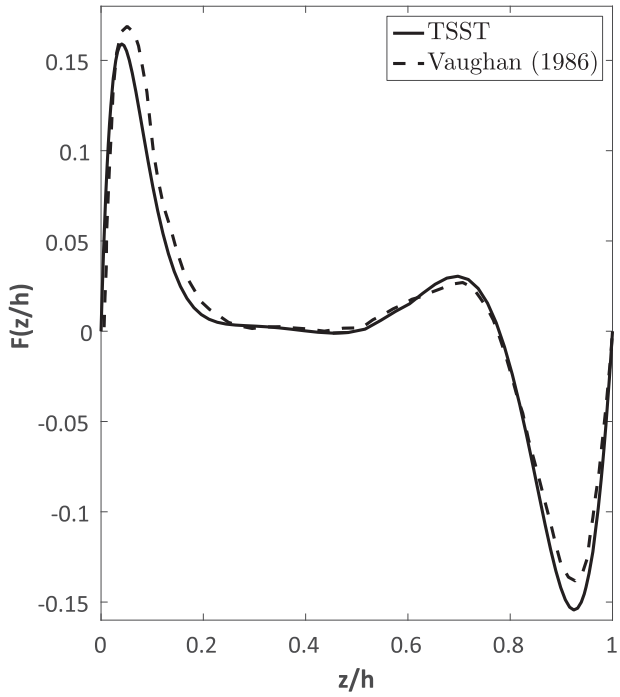

(a) Radial velocity F, at $Re = 112$.

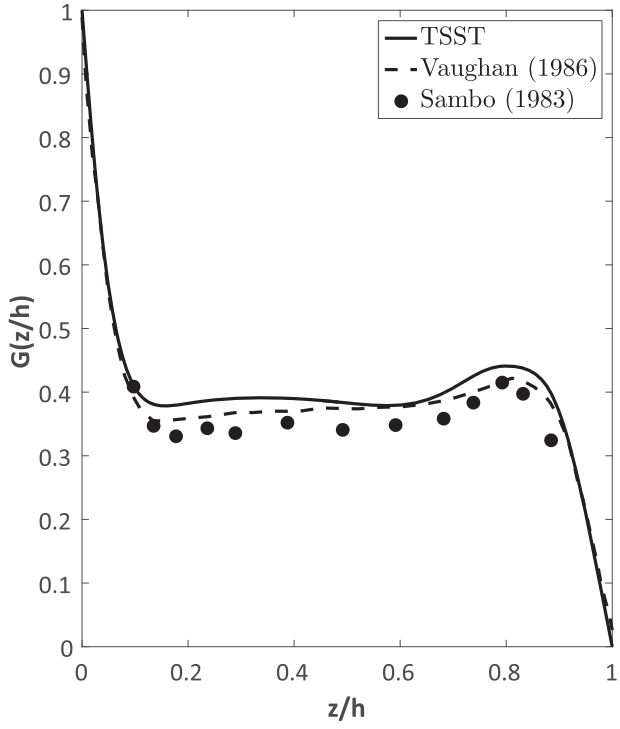

(b) Azimuthal velocity G, at $Re = 134$.

Figure 3. Comparison of the results of the TSST simulation with previous numerical (Vaughan, 1986) and experimental (Sambo, 1983) data ($\mathrm{Re}_\phi = 224$ and $D = 0.1$).

The information on, and results from, these two publications were obtained from Owen and Rogers (1989, p. 138).

The experiments of Sambo (1983) involved an air-based rotor–stator system. The rotor had a radius of $R = 190.5$ mm and the gap width was $h = 19$ mm, giving an aspect ratio of $D = 0.1$. The data were obtained at the radial location $r = 0.5R$ for the radial velocity component and at $r = 0.6R$ for the azimuthal component. The global Reynolds number had a value of $\mathrm{Re}_\phi = 224$. Assuming that the experiments were conducted approximately at a room temperature of 20°C, where the kinematic viscosity of air is $1.51\times10^{-5}\,\mathrm{m^2 s^{-1}}$, this value of Re_ϕ implies a rotational velocity of $\Omega = 20.8\,\mathrm{rad\,s^{-1}}$ equivalent to, approximately, 200 rev/min. This in turn implies local Reynolds numbers of $\mathrm{Re} = 112$ and $\mathrm{Re} = 134$ for the measurement locations associated with the data of, respectively, the radial and the azimuthal velocity components in Figure 3. The flow velocity within the air-filled cavity was measured by means of a Laser-Doppler Anemometry (LDA) system. Vaughan (1986) subsequently developed a finite-difference solver for the Navier–Stokes equations to model the flow within Sambo's system.

Figures 3(a) and 3(b) display a very good qualitative and quantitative agreement between the current TSST simulations and the simulations by Vaughan (1986) for both the radial and the azimuthal flow components. The maximum discrepancies between the results of both models occur near the maxima of the radial flow component, that is near $z/h \approx 0.05$ and $z/h \approx 0.95$, and in the vicinity of $z/h \approx 0.18$ for the azimuthal flow component. Here the differences are of the order of about 1%, or less, for the radial component and approximately 4% for the azimuthal component. Owen and Rogers (1989, p. 138) only display experimental data for the azimuthal flow component from Sambo (1983) and Figure 3(b) reveals that, similar to the results of Vaughan (1986), the present simulations compare well with his experiments.

3.2. Comparison of TSST results with those from the experimental rotor–stator of Colley et al. (2006) and von Kármán flow

Colley et al. (1999, 2006) conducted studies investigating the laminar–turbulent transition over rotating discs spinning with rotational velocity $\Omega = 7.85\,\mathrm{rad\,s^{-1}}$ submerged under water inside a circular tank. The discs had a radius of $R = 0.2\,m$ while the tank had a radius of 0.5 m and a depth of 0.4 m. The distance between the surface of the submerged spinning disc and the liquid surface was approximately 0.15 m. They found that the rotation of their disc induced undesired surface waves with associated wave reflections from the wall of the tank. In attempts to minimize disturbances affecting the boundary-layer flow on their discs, Colley et al. (2006) conducted experiments with two slightly different configurations of their apparatus. In one case the disc was spinning freely under water. In the other case the disc was covered by a lid establishing a configuration resembling the rotor–stator configuration of Figure 1. These configurations are referred to as, respectively, *no-stator* and *stator* in the context of Figures 4 and 5 in this section. Note, however, that in the configuration of Colley et al. (2006) with the lid in place there was a narrow annular gap of about 10–20 mm between the circumferential rim of the rotor disc and the covering shroud. Hence, there may have been some exchange of water through this circumferential gap. The lid was mounted such that the gap width was $h = 0.02$ m, which corresponded to $10\,\delta$ in terms of the boundary-layer thickness over the rotating disc. Neglecting the width of the circumferential gap, the aspect ratio of their facility was hence $D = 0.1$. Colley et al. (2006) conducted hot-film measurements of the radial and azimuthal flow components in the boundary layer over their rotating disc.

The data from Figure 2 in Colley et al. (2006), for both their experimental configurations, are included here in Figures 4 and 5 in comparison with the computational results obtained for TSST simulations and in comparison with the theoretical data based on von Kármán (1921). Figure 4 also includes TSST simulations for $D = 0.092$, $h = 10\delta$ while Figure 5 displays corresponding simulations for $D = 0.918$, $h = 100\delta$. Both figures moreover highlight the Reynolds number dependence by including TSST simulations for $\mathrm{Re} = 210$ and for $\mathrm{Re} = 546$. Here the lower Reynolds number corresponds to a location within the laminar region of the boundary layer while the higher Reynolds number is associated with a location in the turbulent region – i.e. above the critical value near $\mathrm{Re} = 513$ (Lingwood, 1996). Note that there exists no dependence on the Reynolds number for the solution of von Kármán (1921) since it represents a similarity solution expressed in non-dimensional form which is globally valid across the entire laminar-flow region over the rotating disc.

As regards the validation of the TSST approach, the first observation to emerge from a comparison of the data in Figures 4(a), 4(b) and 5(a), 5(b) is that, as regards most aspects, there exists a good qualitative agreement between the TSST simulations, the experimental data of Colley et al. (2006) and the theoretical solution of von Kármán (1921) in all graphs. The only aspect for which agreement is not entirely satisfactory concerns the residual radial motion displayed by the data of Colley et al. (2006) in Figures 4(a) and 5(a), at heights

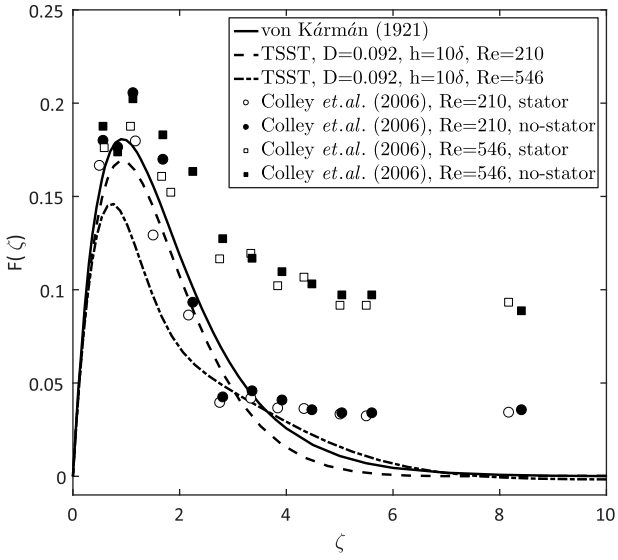

(a) Radial velocity F.

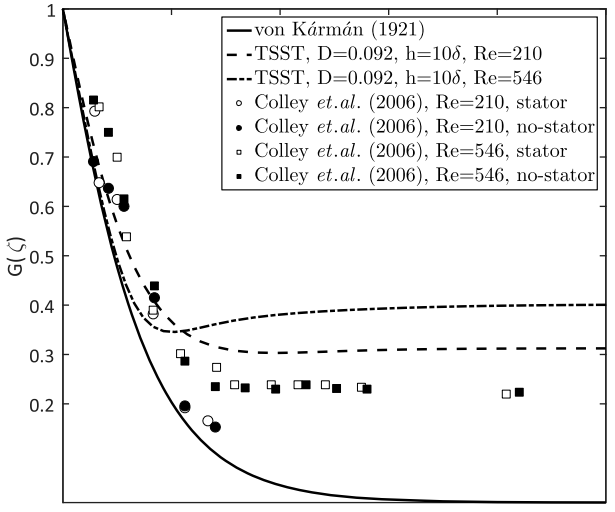

(b) Azimuthal velocity G.

Figure 4. Comparison of the results of the TSST simulations ($D = 0.092$, $h = 10\delta$, $\mathrm{Re}_\phi = 733$, $\mathrm{Re} = 210$ and $\mathrm{Re} = 546$) with the experimental data from Figure 2 in Colley et al. (2006) and the von Kármán (1921) similarity solution.

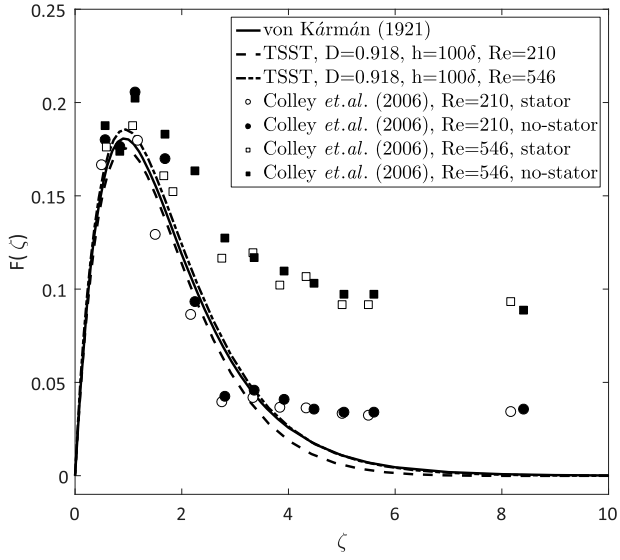

(a) Radial velocity F.

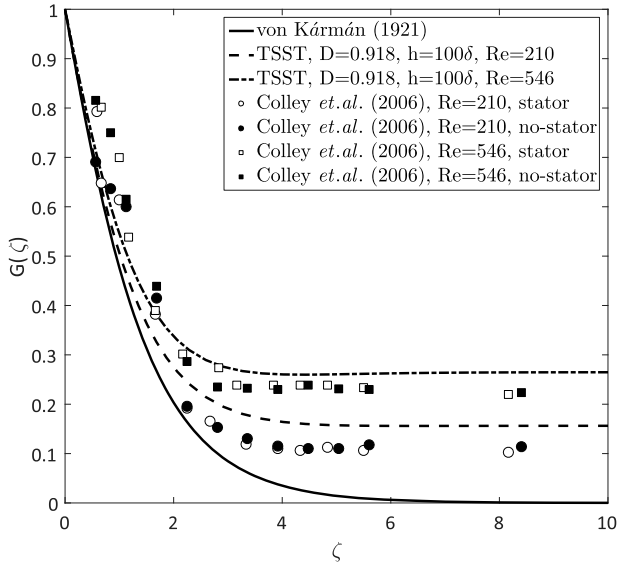

(b) Azimuthal velocity G.

Figure 5. Comparison of the results of the TSST simulations ($D = 0.918$, $h = 100\delta$, $\mathrm{Re}_\phi = 733$, $\mathrm{Re} = 210$ and $\mathrm{Re} = 546$) with the experimental data from Figure 2 in Colley et al. (2006) and the von Kármán (1921) similarity solution.

above ≈ 3. This residual radial motion appears particularly prominent for their experiments at the higher Reynolds number of $\mathrm{Re} = 546$. We are not aware of any other measurements for flow over rotating discs displaying such a prominent residual radial motion. However, it is emphasized that the experimental data of Colley et al. are not suitable to make any definitive quantitative comparisons with the TSST data and the solution of von Kármán. There exist numerous reasons for this. For instance, the circumferential gap between rotor disc and stator in the experiments of Colley et al. may have resulted in alterations of the experimental flow field in comparison with that simulated in the TSST approach. Moreover, in the experiments the hot-film probe is subject to an effect known as yaw-angle bias (Bruun, 1995, p. 71). This arises from along-wire cooling in the flow field with its three velocity components and leads to overestimates of the measured velocity values. The data of Colley et al. (1999, 2006) were not corrected for yaw-angle bias, as discussed in Colley et al. (1999, p. 334), since this was not necessary in the particular context of their studies. Finally, the experiments in the tank of the facility of Colley et al. represents a spatially restricted and, therefore, fairly high-noise environment in which one has to resolve small quantities. To appreciate this,

note that a distance of $\Delta\zeta = 1$ on the abscissa in Figures 4 and 5 corresponds to a vertical height difference of only $\Delta z = 0.36\,mm$ for their experimental data. Similarly, velocity changes of $\Delta F = \Delta G = 0.1$, at $\mathrm{Re} = 210$, correspond to $\Delta u = \Delta v \approx 0.06\,\mathrm{m\,s^{-1}}$ occurring over an interval of only $\Delta\zeta \approx 2$, that is 0.72 mm.

One expects the most favourable agreement between the TSST simulations and von Kármán (1921) for the lowest Reynolds numbers Re and the largest aspect ratio D. Reference to Figure 5 shows that this is indeed the case here where $D = 0.918$, $h = 100\delta$ and for $\mathrm{Re} = 210$. For these parameters a good quantitative agreement is indeed displayed for the radial flow component in Figure 5(a), for all heights ζ and for the azimuthal flow component in Figure 5(b) up to about $\zeta = 2$. For $\zeta > 2$, the azimuthal flow deviates more strongly from von Kármán (1921). However, here the TSST computations are in very good quantitative agreement with the corresponding experimental data by Colley et al. (2006) which show the same type of discrepancy with respect to von Kármán (1921). This type of discrepancy is naturally expected since our simulations and the data of Colley et al. (2006) are for rotor–stator flow whereas the theory by von Kármán (1921) is for a freely spinning disc. Moreover, note that in Figure 5(b) the TSST simulations almost exactly quantitatively mirror the dependence on the Reynolds number that was experimentally observed by Colley et al. (2006).

Besides the above comments relating to the validation of our TSST approach, a comparison with the data in Figures 4(a) and 5(a), and in Figures 4(b) and 5(b), enable a first evaluation of the effects of the aspect ratio D on our TSST simulations, but this will be addressed in more detail in Section 4.1. Nevertheless, these figures furthermore enable an evaluation of the effects of the Reynolds number on the TSST simulations at different values of the aspect ratio D. However, it is not elaborated on this here since it is not relevant in the context of the current study, where the focus is on the comparison of geometry-induced effects and roughness-induced effects.

As an aside to the validation of the TSST approach, the above comparison of the current simulations with the experimental data of Colley et al. (2006) provides the first direct, quantitative support for the speculation expressed in their paper that their data do not approach the similarity solution by von Kármán (1921) for $\zeta \to \infty$ due to residual fluid motion exterior to the boundary layer. In this context, two further brief comments relating to the comparison of the TSST simulations and the data of Colley et al. (2006) are included.

Firstly, the height above the surface of the spinning disc was only about 0.15 m, corresponding to about $h = 76\,\delta$ or $D = 0.75$, for their *no-stator* configuration. Hence, it is not impossible that the effects induced due to the existence of the liquid surface resembled, to some extent, those induced in their rotor–stator-like flow configuration. This may have possibly contributed to the similarity of the experimental data for their *stator* and *no-stator* case. Together with the limited size of the water tank (diameter approx. 1 m) housing the disc (diameter approx. 0.5 m) it may also explain why there exists a residual radial flow motion in Figures 4(a) and 5(a). This is supported by the residual radial flow in Figures 4(a) and 5(a) being more pronounced for the higher local Reynolds number, $\mathrm{Re} = 546$, which corresponds to a position of the hot-film probe closer to the lateral boundary of the water tank and where one would expect stronger effects of any side-wall-induced recirculation flow regions that can result in radial flow.

Secondly, the small quantitative discrepancies between experiment and TSST simulation at $\zeta > 4$ in Figure 5(a), for the parameter configurations that most closely resemble the case of Colley et al. (2006), i.e. $h = 100\,\delta$ or $D = 0.918$ and at $\mathrm{Re} = 210$, are possibly partly associated with the, previously addressed, yaw-angle bias.

3.3. Validation: concluding remarks

In conclusion, the above discussion of the computational simulations involving the TSST approach has demonstrated that these correctly simulate rotor–stator flow and, in particular, the flow within the boundary layer on the rotor disc. Hence, this provides sufficient confidence that the methods are suitable for evaluating qualitative effects, together with their quantitative magnitude, induced by changes in the boundary conditions associated with the rotor–stator configuration. Therewith one can be confident that it is possible to evaluate these effects in comparison with the boundary-layer flow over a freely spinning disc on the basis of the theoretical similarity solution by von Kármán (1921).

The main issues of the current study are now addressed in the following section. Further additional validation of the TSST approach will emerge in Section 5, where the roughness effects predicted on the basis of these computations are compared with the corresponding theoretical results of Cooper et al. (2015), Garrett et al. (2016) and Alveroglu et al. (2016).

4. Results from TSST simulations: geometry effects versus roughness effects

The nature and the magnitude are considered of the effects that variations in the aspect ratio of the rotor–stator system induce on the flow within the boundary layer over the rotor in a rotor–stator system, and

how they compare with roughness-induced effects is evaluated. The underlying rationale being to establish whether the effects in both cases are of similar nature and, if so, whether they must be expected to be of comparable magnitude in the type of system considered here.

4.1. Geometry effects

Figure 6 shows results from TSST simulations illustrating how the aspect ratio D of the rotor–stator system affects the radial and azimuthal components of the flow velocity within the boundary layer on the rotor for a global rotational Reynolds number of $\mathrm{Re}_\phi = 600$ and at a radial position corresponding to a local rotational Reynolds number of $\mathrm{Re} = 500$ (laminar region) – where $R = 0.6\,\mathrm{m}$ and $\Omega = 1\,\mathrm{rad\,s^{-1}}$. Figure 6 shows the computational results from our TSST approach in comparison with the corresponding theoretical laminar velocity profiles of von Kármán (1921) for an unrestricted rotor. The four profiles for the computational results are associated with aspect ratios D of 0.046, 0.092, 0.367 and 0.918. These values for D correspond to gap widths h of 5 δ, 10 δ, 40 δ and 100 δ when expressed in terms of the boundary-layer thickness for the flow over a rotating disc satisfying the theory of von Kármán (1921).

A comparison of the computational profiles in Figure 6 with the curve representing the theory of von Kármán (1921) reveals that, as one would expect, our data approach the results for the freely spinning disc with increasing gap width D. However, even for the aspect ratio $D = 0.918$, corresponding to a gap width of 100 δ, the azimuthal flow component in Figure 6(b) still remains substantially modified in comparison with the von Kármán profile. This is the case at least for all heights above approximately $\zeta = 1$ – and recall that the boundary layer extends to $\zeta = 5.5$ according to von Kármán (1921). At heights above approximately $\zeta = 2$, the difference for the azimuthal flow component is still of the order of $\Delta G \approx 0.15$–0.25, reflecting the core rotation in rotor–stator flow.

In Figure 6(a), the reduction effect of a decreased aspect ratio on the radial flow component is observed especially in the region of approximately $0 \leq \zeta \leq 2$. The reduction in the maximum radial jet flow is in the order of around $\Delta F \approx 0.02$. This corresponds to about 10% in comparison with the value of $F \approx 0.18$ at the position of the maximum. This same sort of reduction effect is also observed as a result of an increase in the geometric roughness height, which will be discussed in the following section. The differences between the rotor–stator flow and the freely spinning disc for the gap width 100 δ are less substantial for the radial flow component than the azimuthal flow component; but, nevertheless, within the region of approximately $3 \leq \zeta \leq 6$, one can still identify differences of up to the order of around $\Delta F \approx 0.003$, which corresponds to about 2% in comparison with the maximum value of $F \approx 0.18$.

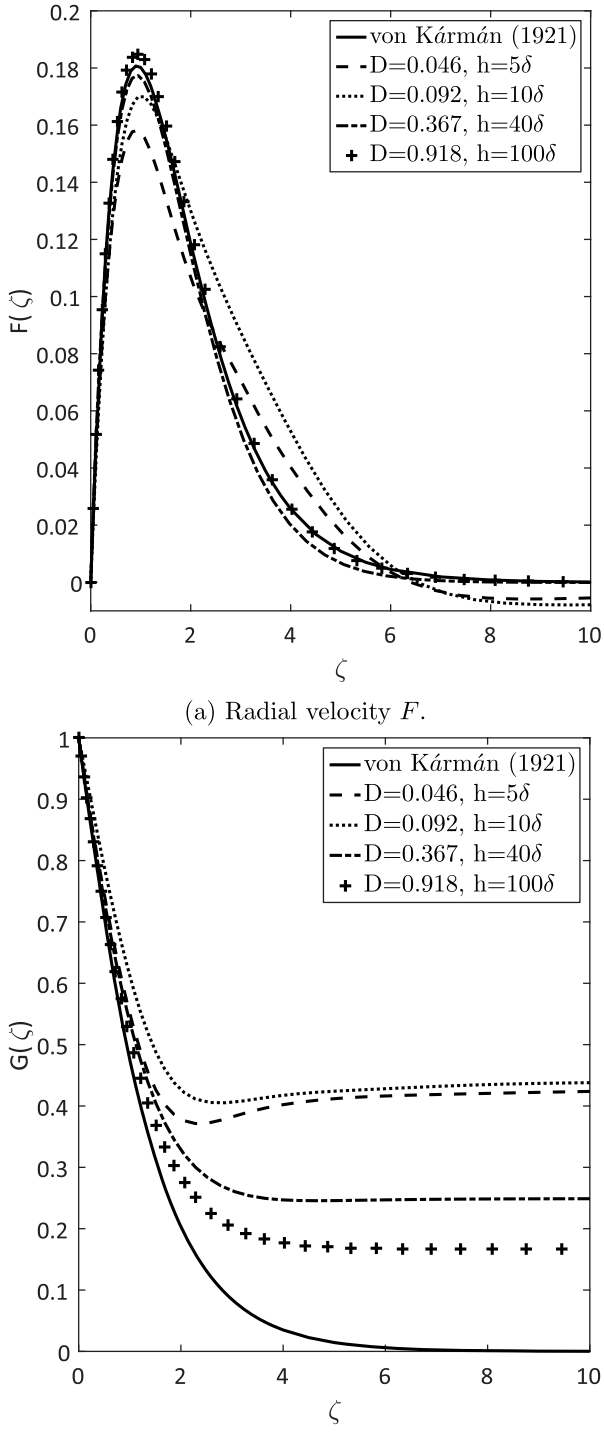

(a) Radial velocity F.

(b) Azimuthal velocity G.

Figure 6. The effect of the aspect ratio on the basic flow profiles ($\mathrm{Re}_\phi = 600$, $\mathrm{Re} = 500$).

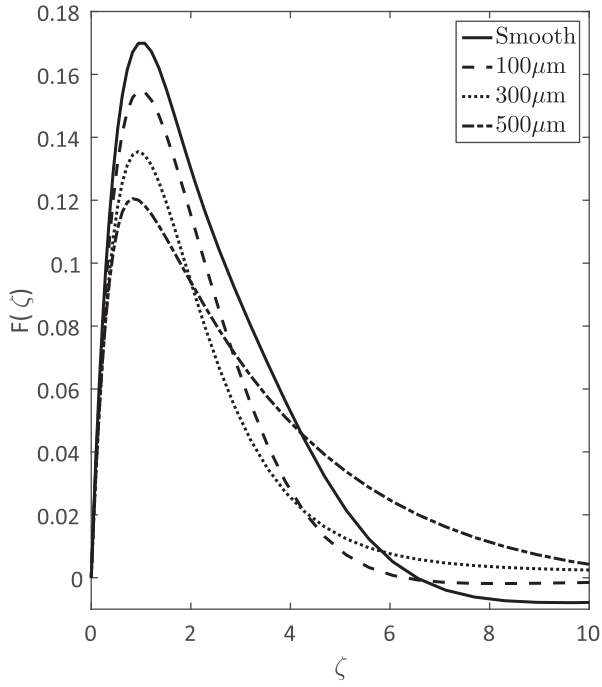

(a) Radial velocity F.

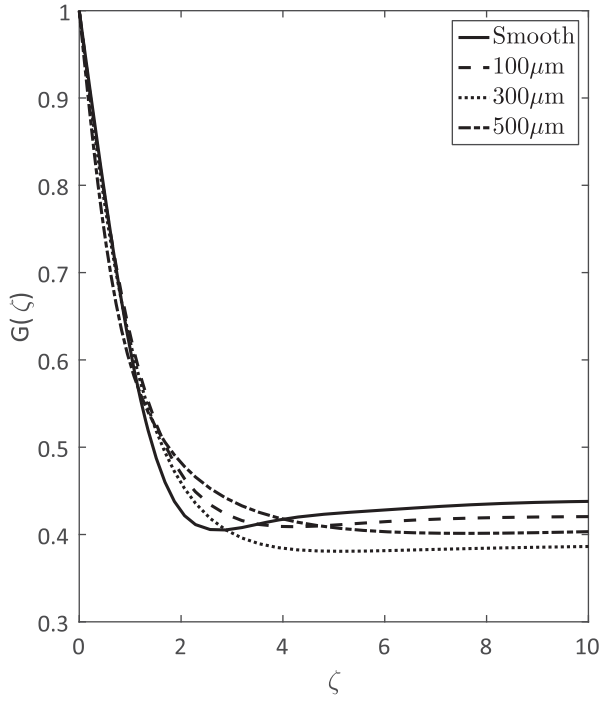

(b) Azimuthal velocity G.

Figure 7. The effect of isotropic roughness on the basic flow profiles ($D = 0.092$, $h = 10\,\delta$, $\mathrm{Re}_\phi = 600$, $\mathrm{Re} = 500$).

4.2. Roughness effects

Figure 7 displays the effects of surface roughness on the radial and azimuthal components of the flow velocity within the boundary layer on the rotor in a rotor–stator configuration as predicted by our TSST approach. The data were obtained for a configuration with an aspect ratio $D = 0.092$ which corresponds to $h = 10\,\delta$, for a global rotational Reynolds number $\mathrm{Re}_\phi = 600$ and for a position associated with a local rotational Reynolds number of $\mathrm{Re} = 500$. The figure compares results for a smooth disc with simulations for values of $K = 100$, 300 and 500 μm for the geometric roughness height (ANSYS®, 2013, p. 75; Schlichting & Gersten, 2004, pp. 526–531). These particular values for the roughness were chosen here since they represent approximately the range of typical roughness heights one would expect to find associated with applications involving drag-reduction techniques in practice.

The inspection of the roughness-induced effects illustrated here in Figure 7 reveals that they are qualitatively similar to the geometry-induced effects in Figure 6 – but a direct comparison to evaluate quantitative difference will be shown in Figure 8. The data in Figure 7(a) reveal that roughness reduces the radial velocity, in comparison with the curve for the smooth disc, within, approximately, $0 \leq \zeta \leq 5$, whereas the trend is reversed for heights above this region.

The magnitude of typical variation of the predictions for different roughness levels are of the order of around $0.02 \leq \Delta F \leq 0.04$ and this is of comparable magnitude to the values $\Delta F \approx 0.02$ obtained for the geometry-induced effects in Figure 6(a).

Similar roughness-induced variations are found for the predictions associated with the azimuthal velocity component in Figure 7(b) where typical values are of the order of around $\Delta G \approx 0.1$ for heights $\zeta > 0.15$, which compares with $0.15 \leq \Delta G \leq 0.25$ for the geometry-induced effects at $\zeta > 2$ in Figure 6(b). Figure 7(b), moreover, shows that roughness is seen to decrease the strength of the core rotation. Although this influence is not directly in line with an increase in roughness, it is of comparable magnitude to the geometry-induced effects.

Thus, the comparison of Figures 7 and 6 indicates that one must expect it to be difficult to distinguish between roughness-induced and geometry-induced effects in experiments. Specifically, and in a general experimental context, the comparison of Figures 7 and 6 defines the required measurement sensitivity for methods aiming to distinguish between geometry-induced and roughness-induced effects in a geometrically restricted environment. Any measurement technology to be adopted must be sufficiently sensitive to resolve velocity changes substantially smaller then the magnitude of the changes expected on the basis of the roughness effects and the geometry effects individually.

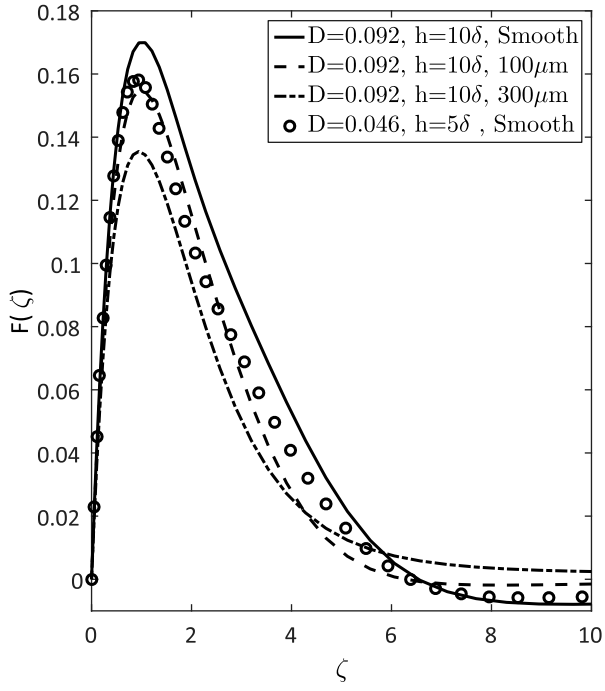

(a) Radial velocity F.

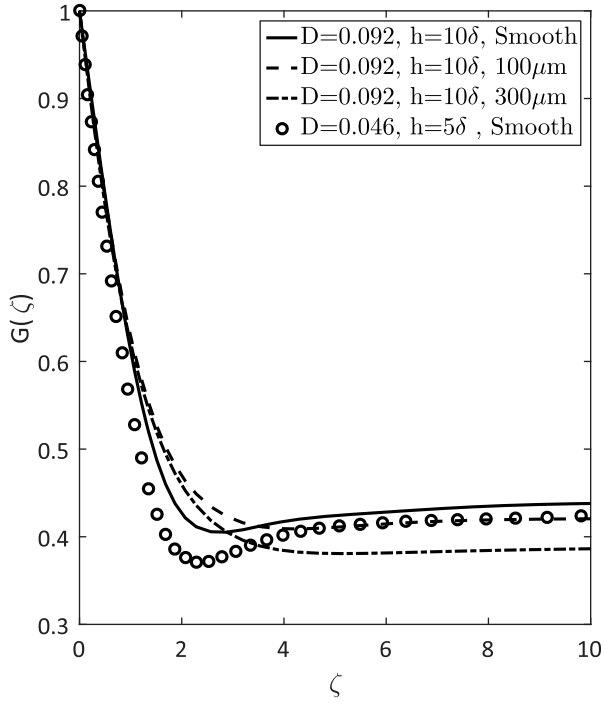

(b) Azimuthal velocity G.

Figure 8. Comparison between the effects of the gap and the roughness ($Re_\phi = 600$, $Re = 500$).

4.3. Comparison: roughness effects versus geometry effects

Figure 8 compares the roughness-induced and the geometry-induced effects, as predicted by the TSST computations, from the preceding two sections to each other. The figure displays results for two aspect ratios $D = 0.046$ and $D = 0.092$, which correspond to $h = 5\,\delta$ and $h = 10\,\delta$, respectively, in comparison with the results for the roughness-induced effects for the largest aspect ratio investigated, $D = 0.092$, $h = 10\,\delta$, with surface roughness of 100 and 300 μm on the stator disc. The figure highlights qualitatively that the predicted roughness-induced effects and the geometry-induced effects on the radial and the azimuthal component of the flow velocity within the boundary layer are very similar in both nature and magnitude.

4.4. Conclusions based on comparison of geometry versus roughness effects from TSST simulations

The main conclusion to be drawn from the comparison of geometry-induced effects and roughness-induced effects in Figures 6, 7 and 8 is that it can be difficult to distinguish between them in a water-based rotor–stator-like rotating disc configuration with typical, practical dimensions similar to those of the facility used in Colley et al. (1999, 2006). Consequently, the predictions based on the TSST simulations suggest that it is difficult to use data from the rotor of such a rotor–stator-like rotating-disc apparatus to corroborate many of the computational predictions for roughness effects induced into the boundary-layer flow for an unrestricted disc spinning in an infinite liquid medium. For this purpose it ideally requires a rotating disc housed within a substantially larger water tank where it can spin freely without the requirement for the stator shroud shown in Figure 1 to eliminate free-surface, wave- and wall-induced disturbances affecting the boundary-layer flow on the surface of the rotating disc.

5. Comparison of predicted roughness effects from TSST simulations with the results of Cooper et al. (2015), Garrett et al. (2016) and Alveroglu et al. (2016)

The roughness-induced effects predicted by the TSST simulations are now compared with the corresponding predictions obtained on the basis of the methods described in detail in Cooper et al. (2015) and in Garrett et al. (2016). The purpose of this comparison is twofold. Firstly, it will provide an additional means of validation for the TSST simulations. Secondly, a favourable comparison between all three fundamentally different approaches will, in turn, yield further support for some of the main conclusions arrived at in Cooper et al. (2015) and Garrett et al. (2016). Note that the TSST simulations in Sections 5.1, 5.2 and 5.3 were obtained for a rotor–stator system of constant gap width, $D = 0.092$,

$h = 10\,\delta$, such that changes of the computational data truly reflect roughness-induced effects only.

The global Reynolds number for the TSST simulations is $\mathrm{Re}_\phi = 600$ and the results are for a radial position corresponding to a local Reynolds number $\mathrm{Re} = 500$. However, the results of Cooper et al. (2015), Garrett et al. (2016) and Alveroglu et al. (2016) are independent of the Reynolds number because in these studies the steady-state flow profiles represent modified versions of the similarity solution of von Kármán (1921) for the Navier–Stokes equations, which describes the flow at all values of the Reynolds number Re.

5.1. TSST versus Cooper et al. (2015)

Figure 9 compares the TSST simulations for roughness-induced effects with corresponding data we obtained on the basis of the methods, and the code, of Cooper et al. (2015). The theoretical considerations and conclusions in that paper are based on the approach of Miklavčič and Wang (2004) whereby roughness is modelled by means of replacing the usual no-slip boundary condition with a *partial slip* condition at the disc surface. In the context of the present study it is only necessary to know that this is achieved by means of introducing two slip coefficients relating the radial and azimuthal velocity components with, respectively, the radial and azimuthal shear stresses. The slip coefficient for the radial component is referred to as λ and that for the azimuthal component is η in Cooper et al. (2015). The *partial slip* reduces to the usual no-slip boundary condition for $\lambda \to 0$ and $\eta \to 0$, whereas the hypothetical condition of complete slip is approached for $\lambda \to \infty$ and $\eta \to \infty$. Hence, higher values for λ and η effectively correspond to rougher surfaces. But note that it is possible to choose $\lambda \neq \eta$ such that rough surfaces of qualitatively different nature can be modelled – for further details refer to Cooper et al. (2015). Based on the *partial slip* condition, they then determine the modified steady-flow velocity field according to the similarity solution of the Navier–Stokes equations due to von Kármán (1921).

Here we select values of $\eta = 0.14$, 0.57 and 1.18 and $\lambda = 0$ to enable a direct inter-comparison between the current TSST results and the results in *both* previous publications, Cooper et al. (2015) and Garrett et al. (2016). As discussed in Garrett et al. (2016), the choice of $\lambda = 0$ was enforced in that study to enable a comparison with Cooper et al. (2015) due to certain limitations of the alternative approach of modelling roughness to be addressed in Section 5.2.

A comparison of the results in Figure 9(a) obtained by means of the TSST simulations for different geometric roughness heights of 100, 300 and 500 μm with the

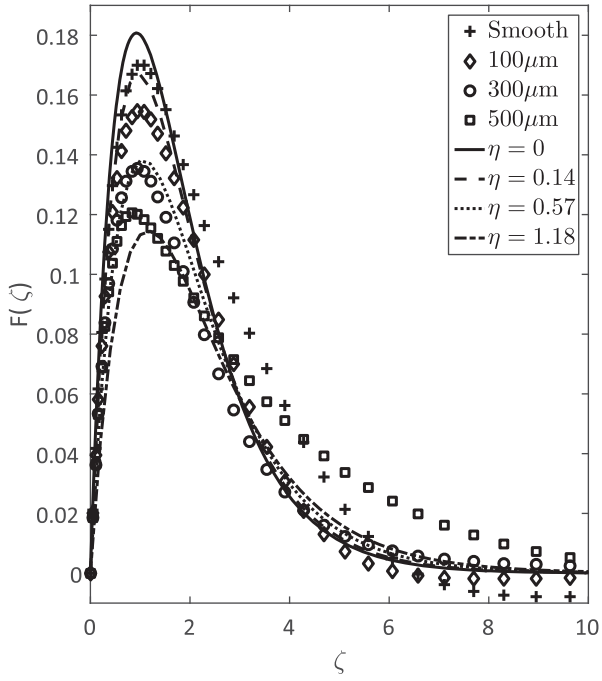

(a) Radial velocity F.

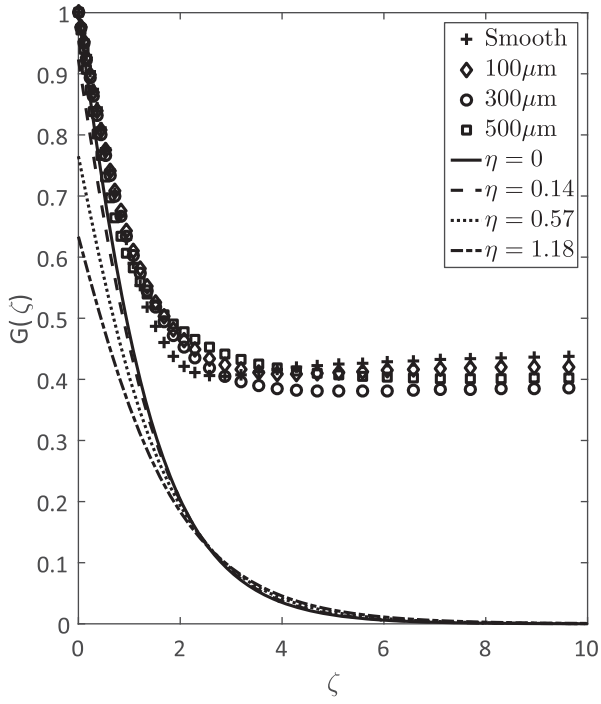

(b) Azimuthal velocity G.

Figure 9. Comparison between the roughness effects predicted by the TSST simulations ($\mathrm{Re}_\phi = 600$, $\mathrm{Re} = 500$) and the roughness effects as predicted by using the code of Cooper et al. (2015) ($\lambda = 0$) based on their *partial slip* approach. Markers identify current TSST data and lines represent data of Cooper et al. (2015).

partial slip approach for the different values of η reveals a very high level of qualitative agreement for the radial velocity component. In this context it is worth highlighting again that it is the instability mode arising from

the inflection point on the radial velocity component (cf. Figure 2) that is primarily responsible for the laminar–turbulent transition of boundary layers with a cross-flow component. Hence, this good agreement between the results of the current TSST approach and Cooper et al. (2015) represents substantial supportive evidence regarding validity of the boundary-layer transition issues discussed in that paper.

A comparison between the roughness-induced effect predicted by the TSST approach and Cooper et al. (2015) is not quite that straightforward for the azimuthal velocity component. This is so since for this component, in Figure 9(b), the transition from rotor–stator flow to rotating-disc flow involves a qualitative change in the velocity profile. In rotor–stator flow there exists rotary flow motion above the boundary layer whereas the azimuthal velocity component vanishes for rotating-disc flow. Hence, the TSST simulations for rotor–stator flow naturally differ quite substantially from those based on the rotating-disc results of Cooper et al. (2015). Nevertheless, what the data in Figure 9(b) do show is that for the TSST simulations and also for the simulations following Cooper et al. (2015) roughness effects are of comparable magnitude.

While partial-slip is a standard approach in modelling flow over rough surfaces, it is however noted that the slip coefficients λ and η associated with the *partial slip* approach do not, a priori, bear any direct relevance to real geometric roughness. In applied contexts they only become useful if, for any particular application, empirical data are available that suggest how their values should be selected. Due to the high level of agreement that the TSST simulations displayed in comparison with experimental and computational data in all preceding sections, and due to the qualitative agreement in the present, and in the following sections, it appears that it may be possible to employ TSST simulations to determine theory-based calibration charts relating λ and η to different values of geometric roughness. However, only future experiments will be able to reveal if this is indeed possible in practice.

5.2. TSST versus Garrett et al. (2016)

Figure 10 compares the TSST simulations for roughness-induced effects from the previous section with corresponding data obtained on the basis of the methods described in detail in Garrett et al. (2016). In that publication, an alternative method of modelling roughness was employed which is based on the approach of Yoon, Hyun & Park (2007). Their approach models roughness by imposing a particular surface distribution as a function of the radial position and assumes a rotational symmetry. The results of Garrett et al. (2016) are shown in terms of the parameter a, which is the ratio of the height to the pitch of the sinusoidal surface roughness. The approach of Yoon et al. (2007) is consequently restricted

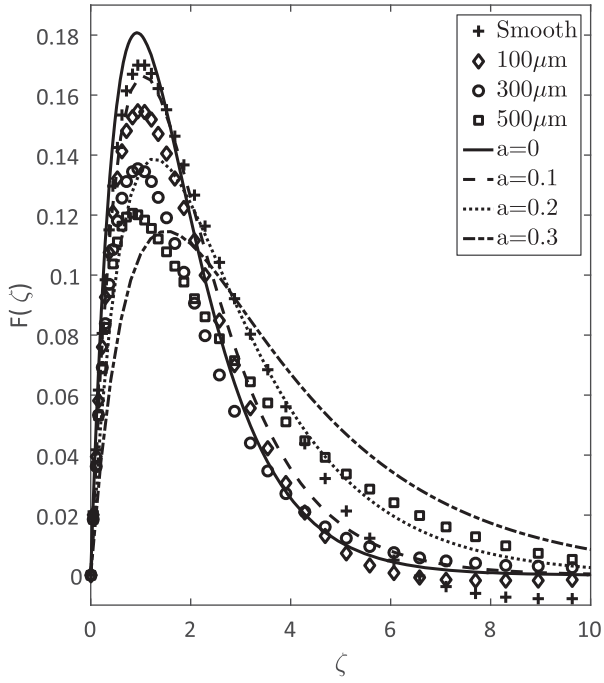

(a) Radial velocity F.

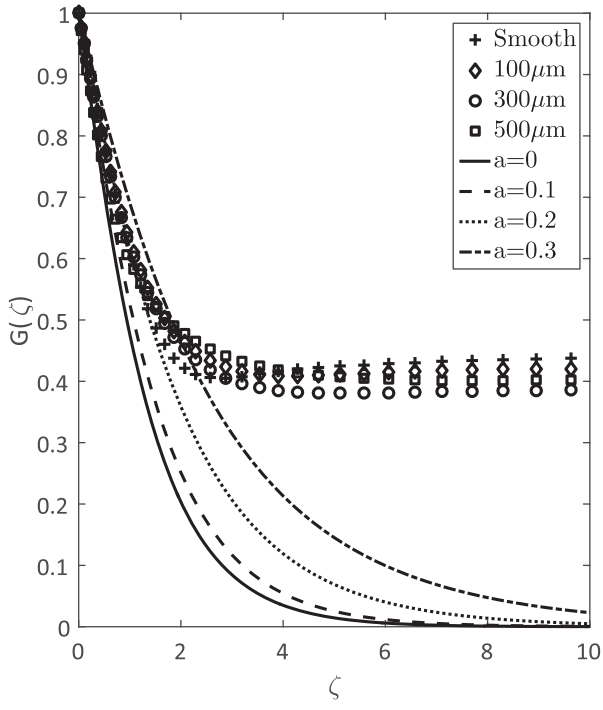

(b) Azimuthal velocity G.

Figure 10. Comparison between the roughness effects predicted by the TSST simulations ($Re_\phi = 600$, $Re = 500$) and the roughness effects predicted in Garrett et al. (2016) based on the approach of modelling roughness by prescribing a surface distribution as a function of the radial position. Markers identify current TSST data and lines represent data of Garrett et al. (2016).

since it models roughness in the radial direction only whereas the more flexible approach based on Miklavčič and Wang (2004) in Cooper et al. (2015) allowed for modelling roughness in both the radial and the azimuthal directions by means of selecting the slip coefficients λ and η as desired. This limitation of the approach by Yoon et al. (2007) is the reason that the value $\lambda = 0$ had to be chosen in the previous section. The data in Figures 10(a) and 10(b) do not require a further detailed description since they exactly mirror the observations discussed in connection with Figures 9(a) and 9(b) in the preceding section. It is, however, emphasized again that it is not permissible to make quantitative comparisons between the results obtained from the different simulation approaches due to the discussed specific differences, and limitations, associated with the methods in Cooper et al. (2015) and Garrett et al. (2016). The important result is that all approaches lead to consistent qualitative trends and to changes of the relevant quantities which are of similar magnitude.

5.3. TSST versus Alveroglu et al. (2016)

The type of steady-state, base-flow velocity profiles discussed in the preceding sections are underlying the boundary-layer stability analysis summarized in Cooper et al. (2015) and in Garrett et al. (2016), where results for different types and levels of roughness are considered. Boundary-layer stability issues are not the focus of the current study, which compares roughness-induced and confinement-induced effects on the steady-state base-flow profiles only. Nevertheless, as part of the current study the base profiles obtained here for the rotor disc were subjected to a stability analysis. This led to an observation of particular interest and significance as regards rotating-disc flow in general and in relation to the very recent roughness-related boundary-layer-stability considerations of Alveroglu et al. (2016) for the BEK family of flows. Since a comparable observation does not seem to have been reported previously anywhere in the rotating-disc literature it is briefly documented here.

Alveroglu et al. (2016) modelled roughness based on the approach of Miklavčič and Wang (2004) and by applying the same methods as in Cooper et al. (2015). Figure 11 compares the neutral stability curves obtained by our TSST simulations with curves of Alveroglu et al. (2016). The figure shows the standard type of results where the wave-number of the radial disturbance α_r is displayed as a function of the local Reynolds number Re. For any value of Re, any particular disturbance α_r is unstable if it lies within the area enclosed by the curves displayed and it is stable if it lies outside the area enclosed. The figure shows the TSST simulations in comparison with

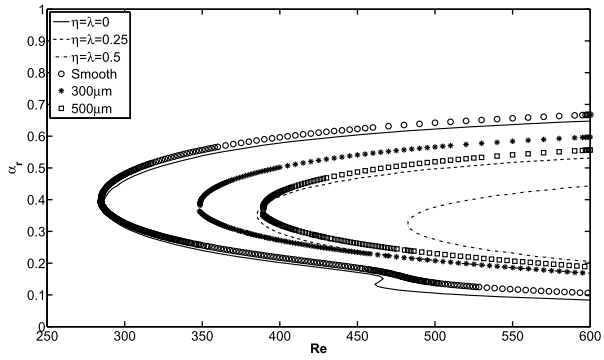

(a) von Kármán flow configuration.

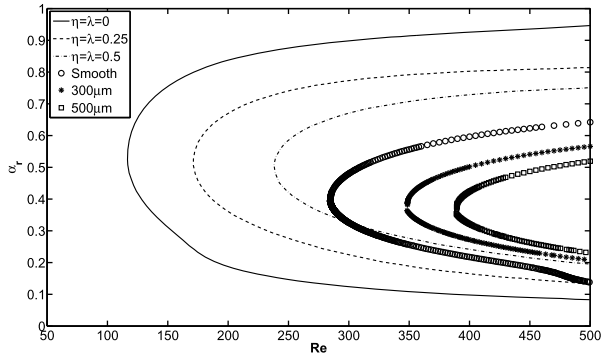

(b) Ekman flow configuration.

Figure 11. Comparison of neutral curves obtained by the TSST simulations for the rotor–stator flow configuration with the ones presented by Alveroglu et al. (2016) for isotropic roughness. Markers identify results of stability calculations based on current TSST data and lines represent data of Alveroglu et al. (2016).

data of Alveroglu et al. (2016) for rotor–stator Kármán and Ekman flow over isotropically rough discs. These two flow cases were selected from Alveroglu et al. (2016) for the comparison because the qualitative nature of the flow over the rotor-disc in the rotor–stator cavity flow lies somewhat between these two types of flow scenario.

The main issue addressed here relates to one of the two convective instability modes for rotating-disc flow which are referred to as Type I and Type II modes in the literature (Lingwood & Alfredsson, 2015; Reed & Saric, 1989; Saric et al., 2003)The Type I mode is a viscous instability arising due to Rayleigh's inflection point criterion (Schlichting & Gersten, 2004, p. 432) and as a consequence of the existence of the inflection point on the velocity profile of the radial component of the flow velocity in Figure 2. The Type II mode is an inviscid instability associated with streamline curvature and Coriolis effects. The Type I mode reveals itself in experiments in the form of a series of co-rotating vortices within the laminar–turbulent transition region of the boundary layer over the disc and it constitutes the dominant mode leading to transition. However, the exact physical nature of the Type II mode remains, as yet, unknown. The result documented below, together with in-depth further TSST

simulations, might be able to shed more light on the exact physical nature of the Type II mode.

In both Figures 11(a) and 11(b), there is a qualitative agreement between the results showing a stabilizing effect of roughness on both the inviscid Type I (cross-flow) and the viscous Type II instability mode. Stabilization is revealed by a shift of the curves towards higher Reynolds number; i.e. a shift to the right in the figure. It is emphasized that it is not possible to make quantitative comparisons between the present results for rough discs and those of Alveroglu et al. (2016). This is due to the approach of Miklavčič and Wang (2004), adapted by Alveroglu et al. (2016), being based on two *ad hoc* slip coefficients, introduced into Newton's law of viscosity, to simulate partial slip at the disc surface in the radial and azimuthal directions. These slip coefficients have no, *a priori*, immediate relation to the real physical roughness height as prescribed in the context of the current TSST simulations.

Note, nevertheless, that for the von Kármán flow over smooth surfaces in Figure 11(a) there exists a very good quantitative agreement between the results for the neutral-stability curves obtained from the TSST simulations and the corresponding computations of Alveroglu et al. (2016). Both sets of results are in almost perfect agreement with each other, apart from the absence of the Type II instability in the current TSST simulation within the narrow region around $460 \leq \mathrm{Re} \leq 480$ where $0.13 \leq \alpha_r \leq 0.15$. The Type II mode is represented by the little kink on the curve for $\eta = \lambda = 0$ in that parameter region. The very good quantitative agreement between the neutral-stability curves found here further reinforces confidence in the TSST simulations. In fact, the close agreement suggests that it may even become possible to employ TSST simulations to calibrate the slip coefficients, when used in the context of the type of calculations described in Cooper et al. (2015) and Alveroglu et al. (2016), for subsequent comparisons with experimental data. The main result of this section relates, however, to the absence of the Type II mode for the TSST results.

In Figure 11(a) the Type II mode was absent for the current TSST simulations of rotor–stator cavity flow over a smooth disc. Reference to Figure 11(b) reveals that the Type II mode also vanishes for the results of Alveroglu et al. (2016) for Ekman flow displayed there. This correspondence suggests that the absence of the Type II mode from the TSST simulations in Figure 11(a) reflects the fact that the flow over the rotor disc of the rotor–stator arrangement represents an intermediate state between the limits of von Kármán flow and Ekman flow. Hence, it suggests that the absence of the Type II mode for the TSST simulations is brought about by the non-vanishing fluid motion in the core of the flow field between the two boundary layers on the rotor and the stator. Since the complete data for the entire three-dimensional flow field are available for the TSST results, which is in contrast to the situation for the results of Alveroglu et al. (2016), it may be possible that a detailed, careful examination of TSST data can shed more light on what features of the flow field exactly lead to the disappearance of the Type II mode during the transition from von Kármán flow to Ekman flow. To assist with the evaluation of the stability issues addressed above in a broader context we would, in conclusion, also like to draw attention to Table III in the appendix of Garrett et al. (2016), where a literature survey of the critical instability parameters associated with flow over smooth rotating discs is presented.

6. Summary and conclusion

A computational study investigating the boundary-layer flow on the rotor inside the enclosed cavity of a rotor–stator system was presented. The main focus was on the individual effects that the surface roughness and aspect ratio, $D = h/R$, of the system induce on the boundary-layer flow above the rotor. These effects were compared with corresponding roughness-induced effects in the boundary layer over a freely spinning, unrestricted disc, the latter being the limiting case of rotor–stator flow approached for $R \to \infty$ and $h \to \infty$ for which a similarity solution to the Navier–Stokes equations exists, which was obtained by von Kármán (1921).

The study was conducted by means of the TSST approach within the ANSYS® Fluent® software package. The simulations were validated against previous experimental data (Colley et al., 1999, 2006; Sambo 1983), and computational data (Vaughan, 1986) and evaluated further for consistency in the context of the recent theoretical considerations summarized in Cooper et al. (2015), Garrett et al. (2016) and Alveroglu et al. (2016). A very good qualitative and quantitative level of agreement between the current simulations and the existing previous work was found.

The original motivation for the study rested on the intent to evaluate the nature and the magnitude of roughness-induced and geometry-induced effects in a rotor–stator flow to establish whether it would be possible to distinguish between them in our existing rotating disc facility. However, the results obtained lead to conclusions which are of relevance in a substantially wider context.

In particular, a high level of consistency between the roughness-induced effects predicted on the basis of the TSST simulations and the corresponding theoretical results of Cooper et al. (2015) and Garrett

et al. (2016) was obtained. This leads to a very important general, overall conclusion. The methods underlying the TSST approach to model roughness effects rely strongly on input parameters obtained from experimental data obtained by other authors in entirely different experimental scenarios compared with those considered here. In contrast, the other two studies model roughness in terms of some very simple theoretical assumptions. The fact that all approaches yield results which are, overall, mutually consistent gives confidence in the validity of the qualitative behaviours observed. Due to the details associated with the methods adopted to model roughness in Cooper et al. (2015) and Garrett et al. (2016), a quantitative agreement between their results and those of the current study is, however, not possible.

Specifically, the fact that the TSST approach reconfirms that roughness is expected to stabilize the Type I instability mode is very important in a general context. The Type I mode is the dominant mode resulting in the laminar–turbulent transition of boundary layers with a cross-flow component, as encountered in similar form, for instance, over highly swept aircraft wings. Stabilization of the Type I mode equates to postponed transition and, therewith, to reduced skin-friction drag. Hence, the results of the TSST computations are strongly reassuring in that surface roughness can be used in the context of the development on new passive drag-reduction techniques as suggested by the results of Cooper et al. (2015) and Garrett et al. (2016). The TSST results therewith also provide indirect support to the further results contained in Cooper et al. (2015) and Garrett et al. (2016), which were not discussed here, that point a way forwards towards theory-led strategies for the design of energetically-optimized, transition-delaying surface roughness.

Moreover, the consistency in the comparisons also extended across the different BEK flow scenarios investigated. It was discussed that our rotor–stator flow can be considered as an intermediate state between von Kármán flow and Ekman flow. For the case of rotor–stator flow over a smooth disc a very good quantitative agreement between the neutral stability curve obtained by our TSST simulations and the corresponding curve for von Kármán flow of Alveroglu et al. (2016) was found. The results only differed in a narrow Reynolds-number range where the results for rotor–stator flow revealed the disappearance of the Type II instability mode. Nevertheless, the disappearance of this mode is also observed by Alveroglu et al. (2016) for Ekman flow in the same Reynolds number regime. This led to the conclusion that the absence of the Type II mode for the TSST simulations arises as a consequence of the non-vanishing fluid motion in the core of the flow field between the two boundary layers on the rotor and the stator.

Finally, as regards the original motivation and goal of the study, the results have revealed that the effects induced by changes in the geometric boundary conditions in a rotor–stator facility can be of similar nature and magnitude as the effects induced by roughness. While only one particular system was investigated here, the result nevertheless suggests that there probably exist other flow configurations – related to the present one or not – where roughness-induced and geometry-induced effects may compete with each other in a similar manner and where this may have to be taken into consideration in the context of the particular scientific problems studied or the design aspects addressed.

Disclosure statement

No potential conflict of interest was reported by the authors.

Funding

MÖ wishes to acknowledge financial support from the Ministry of National Education of the Republic of Turkey; SJG is supported by a Senior Fellowship of the Royal Academy of Engineering, funded by the Leverhulme Trust.

Nomenclature

a	the ratio of the height to the pitch of the sinusoidal roughness
D	aspect ratio; $= \frac{h}{R}$
$F(\zeta)$	non-dimensional radial velocity; $= \frac{u}{\Omega r}$
$G(\zeta)$	non-dimensional azimuthal velocity; $= \frac{v}{\Omega r}$
h	gap between rotor and stator, (m)
$H(\zeta)$	non-dimensional axial velocity; $= \frac{w}{\sqrt{\nu\Omega}}$
k	turbulence kinetic energy, $\left(m^2/s^2\right)$
K	geometric roughness height, (m)
K_s	equivalent sand grain roughness
r	radial coordinate, (m)
R	radius of the rotor–stator system, (m)
Re	local rotational Reynolds number; $= \sqrt{\frac{\Omega r^2}{\nu}}$
Re_ϕ	global rotational Reynolds number; $= \sqrt{\frac{\Omega R^2}{\nu}}$
$\tilde{\mathrm{Re}}_{\Theta t}$	momentum–thickness Reynolds number; $= \frac{U\delta_2}{\nu}$
u	radial velocity, (m/s)
U	local velocity, (m/s)
v	azimuthal velocity, (m/s)
y^+	dimensionless wall distance
w	axial velocity, (m/s)
z	axial coordinate, (m)
γ	intermittency
δ	boundary layer thickness, m; $= 5.5\delta^*$
δ_2	momentum–thickness, m

δ^*	characteristic length scale, m; $= \sqrt{\frac{\nu}{\Omega}}$
ϵ	the rate of dissipation of the turbulence kinetic energy, (m^2/s^3)
ζ	non-dimensional axial coordinate; $= \frac{z}{\delta^*}$
η	the azimuthal component of the slip coefficient
θ	azimuthal coordinate
λ	the radial component of the slip coefficient
ν	kinematic viscosity, (m^2/s)
Ω	angular velocity, (rad/s)
ω	the specific rate of dissipation of the turbulence kinetic energy, $(1/s)$
α_r	the wave-number of the radial disturbance
LDA	Laser-Doppler Anemometry
BEK	Bödewadt, Ekman, von Kármán
LES	Large Eddy Simulation
SST	Shear Stress Transport
TSST	Transition Shear Stress Transport
CFD	Computational Fluid Dynamics

ORCID

M. Özkan http://orcid.org/0000-0002-0770-1219

References

Aldaş, K., & Yapıcı R. (2014). Investigation of effects of scale and surface roughness on efficiency of water jet pumps using CFD. *Engineering Applications of Computational Fluid Mechanics*, *8*, 14–25. doi:10.1080/19942060.2014.11015494

Alveroglu, B., Segalini, A., & Garrett, S. (2016). The effect of surface roughness on the convective instability of the BEK family of boundary-layer flows. *European Journal of Mechanics – B/Fluids,*, *56*, 178–187. doi:10.1016/j.euromechflu.2015.11.013

ANSYS, (2013). *ANSYS Fluent Theory Guide, Release 15.0.* Canonsburg, PA: ANSYS.

Bruun, H. H. (1995). *Hot-wire anemometry, principles and signal analysis*. Oxford, UK: Oxford University Press.

Colley, A. J., Carpenter, P. W., Thomas, P. J., Ali, R., & Zoueshtiagh, F. (2006). Experimental verification of Type-II-eigenmode destabilization in the boundary layer over a compliant rotating disk. *Physics of Fluids*, *18*. doi:10.1063/1.2202175

Colley, A. J., Thomas, P. J., Carpenter, P. W., & Cooper, A. J. (1999). An experimental study of boundary-layer transition over a rotating, compliant disk. *Physics of Fluids*, *11*, 3340–3352. doi:10.1063/1.870193

Cooper, A. J., Harris, J. H., Garrett, S. J., Özkan, M., & Thomas, P. J. (2015). The effect of anisotropic and isotropic roughness on the convective stability of the rotating disk boundary layer. *Physics of Fluids*, 27. doi:10.1063/1.4906091

Garrett, S. J., Cooper, A. J., Harris, J. H., Ozkan, M., Segalini, A., & Thomas, P. J. (2016). On the stability of von Kármán rotating-disk boundary layers with radial anisotropic surface roughness. *Physics of Fluids*, 28. doi:10.1063/1.4939793

Kármán, T. V. (1921). Über laminare und turbulente Reibung. *ZAMM – Journal of Applied Mathematics and Mechanics/Zeitschrift für Angewandte Mathematik und Mechanik*, *1*, 233–252. doi:10.1002/zamm.19210010401

Langtry, R. B., & Menter, F. R. (2009). Correlation-based transition modeling for unstructured parallelized computational fluid dynamics codes. *AIAA Journal*, *47*, 2894–2906. doi:10.2514/1.42362

Launder, B., Poncet, S., & Serre, E. (2010). Laminar, transitional, and turbulent flows in rotor–stator cavities. *Annual Review of Fluid Mechanics*, *42*, 229–248. doi:10.1146/annurev-fluid-121108-145514

Lingwood, R. J. (1996). An experimental study of absolute instability of the rotating-disk boundary-layer flow. *Journal of Fluid Mechanics*, *314*, 373–405. doi:10.1017/S0022112096000365

Lingwood, R. J., & Alfredsson, P. H. (2015). Instabilities of the von Kármán boundary layer. *Applied Mechanics Reviews*, 67. doi:10.1115/1.4029605

Menter, F. R. (1994). 2-Equation eddy-viscosity turbulence models for engineering applications. *AIAA Journal*, *32*, 1598–1605. doi:10.2514/3.12149

Menter, F. R., Langtry, R. B., Likki, S. R., Suzen, Y. B., Huang, P. G., & Volker, S. (2006). A correlation-based transition model using local variables – Part I: Model formulation. *Journal of Turbomachinery – Transactions of the ASME*, *128*, 413–422. doi:10.1115/1.2184352

Miklavčič, M., & Wang, C. Y. (2003). The flow due to a rough rotating disk. *Zeitschrift fur Angewandte Mathematik und Physik*, *55*, 235–246. doi:10.1007/s00033-003-2096-6

Owen, J. M., & Rogers, R. H. (1989). *Flow and heat transfer in rotating disc systems – Vol. 1: Rotor–stator systems*. Taunton, UK: Research Studies Press.

Reed, H. L., & Saric, W. S. (1989). Stability of three-dimensional boundary layers. *Annual Review of Fluid Mechanics*, *21*, 235–284. doi:10.1146/annurev.fl.21.010189.001315

Sambo, A. S. (1983). *A theoretical and experimental study of the flow between a rotating and a stationary disc* (Unpublished doctoral dissertation). University of Sussex. Brighton, UK.

Saric, W. S., Reed, H. L., & White, E. B. (2003). Stability and transition of three-dimensional boundary layers. *Annual Review of Fluid Mechanics*, *35*, 413–440. doi:10.1146/annurev.fluid.35.101101.161045

Schlichting, H., & Gersten, K. (2004). *Boundary layer theory* (8th ed.). New York: Springer.

Vaughan, C. (1986). *A numerical investigation into the effect of an external flow field on the sealing of a rotor–stator cavity* (Unpublished doctoral dissertation). University of Sussex. Brighton, UK.

Yoon, M. S., Hyun, J. M., & Park, J. S. (2007). Flow and heat transfer over a rotating disk with surface roughness. *International Journal of Heat and Fluid Flow*, *28*, 262–267. doi:10.1016/j.ijheatfluidflow.2006.04.008